Atom Indonesia

Journal homepage: https://atomindonesia.brin.go.id

Seismic Risk Analysis of the Serpong Nuclear Complex and the RSG-GAS Reactor Using Microseismic Methods

A. Satriyo[1,2*], W. Suryanto[2], T. Anggono[3], M. Subekti[1], Sucipta[4], J. Jatnika[5], R. Swastikarani[6], N. Sugianto[7]

[1]*Directorate for Nuclear Facility Management, National Research and Inovation Agency, Jakarta 10340, Indonesia*
[2]*Department of Mathematics and Natural Sciences, University of Gadjah Mada, Yogyakarta 55281, Indonesia*
[3]*Research Center for Geological Disaster, National Research and Inovation Agency, Bandung 40135, Indonesia*
[4]*Research Center for Nuclear Material and Radioactive Waste Technology, National Research and Inovation Agency, South Tangerang 15314, Indonesia*
[5]*Bandung Geophysics Station, Meteorological, Climatological, and Geophysical Agency, Bandung 40161, Indonesia*
[6]*Center for Engineering Seismology, Potential Geophysics, and Time Mark - Meteorological, Climatological, and Geophysical Agency, Jakarta 10720, Indonesia*
[7]*Geophysics, Matematics and Natural Sciences - University of Bengkulu, Bengkulu 38371, Indonesia*

ARTICLE INFO

Article history:
Received 23 December 2024
Received in revised form 27 April 2025
Accepted 26 May 2025

Keywords:
Serpong Nuclear Complex (SNC)
Reactor RSG-GAS
Horizontal to Vertical Spectral Ratio (HVSR)
Floor Spectral Ratio (FSR)
Peak Ground Acceleration (PGA)

ABSTRACT

The G.A. Siwabessy research reactor (RSG-GAS), located in the Serpong Nuclear Complex (SNC), is a critical component of Indonesia's nuclear research infrastructure. This study aims to assess the seismic safety of the RSG-GAS reactor and its surrounding complex using microseismic methods, specifically the Horizontal-to-Vertical Spectral Ratio (HVSR) and Floor Spectral Ratio (FSR) techniques. HVSR measurements conducted across the B. J. Habibie Science and Technology Area (KST) revealed an average natural frequency (f_0) of 3.49 Hz (range: 2.84-4.43 Hz), amplification factors (A_0) averaging 2.84 (range: 2.11-4.88), and seismic susceptibility indices (Kg) averaging 2.72 (range: 1.34-4.39). The HK9 site, positioned 124 meters from the reactor, exhibited lower-than-average values, indicating reduced seismic vulnerability in the immediate reactor vicinity. FSR analysis was conducted to evaluate key structural parameters, including the Resonance Index (IR), inter-level deviation (γ_i), peak ground acceleration (αb_i), and Building Vulnerability Index (Ktg_i). Most IR values fell within the medium-risk range (20.07 %-22.63 %), while one measurement point recorded 3.98 %, indicating high resonance risk. Inter-level deviations remained within acceptable safety thresholds; however, peak ground acceleration values exceeded critical limits at several levels, most notably at FU8 where 272.63 gal was recorded at -6.5 m elevation-significantly surpassing established safety standards. Several Building Vulnerability Index values also exceeded recommended safety limits. The findings demonstrate that while the RSG-GAS facility generally exhibits low-to-moderate seismic amplification and structural vulnerability, targeted structural reinforcements are essential at critical locations, particularly at the FU8 level. This study provides a comprehensive framework for enhancing seismic resilience of nuclear facilities in seismically active regions and contributes to the long-term safety assessment protocols for Indonesia's nuclear infrastructure.

INTRODUCTION

Nuclear facility development in Indonesia began in the 1950s, with significant advancement occurring in the 1980s through the establishment of the Serpong Nuclear Complex (SNC), now known as the B. J. Habibie Science and Technology Area (KST B. J. Habibie) at Tangerang Selatan in 2020. This complex houses several critical installations, including the Radioisotope Radiopharmaceutical Production Factory (ITRR), Nuclear Fuel Installation (IBBN), Radioactive Waste Treatment Plant (IPLR), and the G.A. Siwabessy Multipurpose

*Corresponding author.
E-mail address: andromeda.ardhane@gmail.com
DOI: https://doi.org/10.55981/aij.2025.1596

Reactor Installation (IRSG or RSG-GAS reactor) (Fig. 1). The presence of nuclear facilities often evokes public concern, particularly among nearby residents, whose sense of security was deeply shaken by the Fukushima Daiichi accident in March 2011 [1]. The RSG-GAS reactor, operating at 30 MW thermal power, consists of two main structures: the reactor building and the staircase building, which serves as a supporting facility.

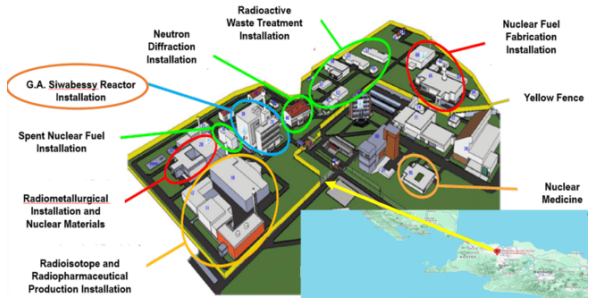

Fig. 1. Overview of the layout of the Serpong Nuclear Complex (SNC), which is the largest nuclear area in Indonesia.

Ensuring long-term safety and reliability of nuclear infrastructure requires continuous evaluation of structural and geotechnical conditions. Prolonged operation, aging, and external factors such as neutron irradiation, thermal stress, mechanical fatigue, and corrosion progressively degrade reactor systems and structures [2]. The 2019 comprehensive inspection of the RSG-GAS facility revealed significant structural deterioration, including cracks, spalling, corrosion, and water seepage damage across multiple building levels [3]. These findings documented various types of structural damage (Table 1) with a total of 52 wall damages, 31 floor damages, and concrete reinforcement corrosion at the -6.5 m level distributed across different building elevations (Table 2). Examples of structural damage, including cracks in walls, floor ruptures, and reinforcement corrosion, are illustrated in Fig. 2. The reactor building is continuously subjected to vibrations from internal sources, such as pumps in the air ventilation system and the reactor pre-oxidation system, as well as from external vibrating systems located outside the reactor building [3].

Table 1. Type of structural damage to the RSG-GAS reactor building identified during the 2019 inspection.

No	Types of Concrete Structure Damage	Exist	Condition
1.	Crack	Yes	Cracks in wall structures and floor plates
2.	Crop	No	Good condition
3.	Spalling	Yes	Spalling wall structures and floor plates
4.	Corrosion of concrete bones	Yes	Concrete reinforcement steel at the level of -6.5 m
5.	Settlement	No	Good condition
6.	Horizontal displacement	No	Good condition
7	Abraded/eroded	No	Good condition

Table 2. The number of damages that occurred inside the reactor building during the 2019 inspection.

Level / Altitude (meters)	Wall	Floor	Concrete Bone
-6.50	10	1	1
0	5	9	-
8	5	6	-
13	4	-	-
17.40	9	5	-
23	1	1	-
26.60	18	9	-
SUM	52	31	1

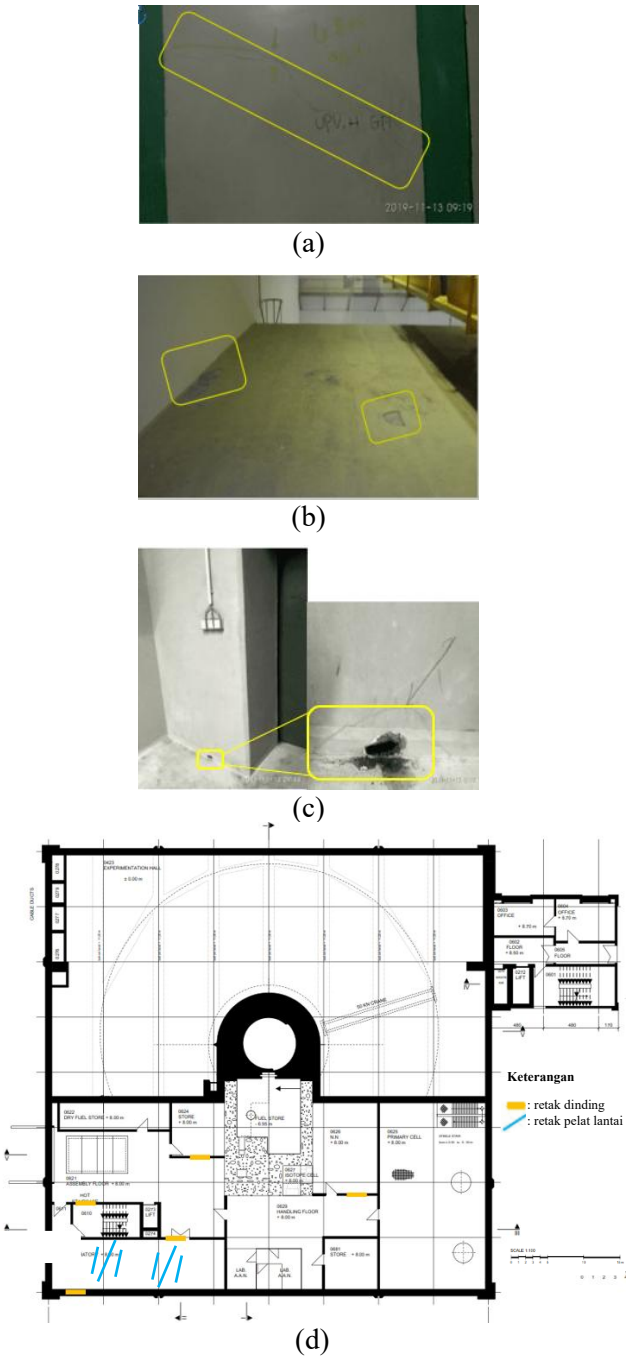

Fig. 2. (a) Structural cracks in the walls at the 8 meters level, (b) Floor damage in the form of ruptures and structural cracks at the of 26.60 meters level, (c) Corrosion of concrete reinforcement steel observed in one of the rooms at the -6.50 meters level, (d) Distribution of damage at the 8 meters level of the reactor building. Yellow box indicates the wall damage, while light blue line represents floor damage.

Indonesia's location within the tectonically active Ring of Fire exposes nuclear facilities to substantial seismic risks. The SNC faces threats from both subduction-related earthquakes along the Sumatra-Java trench and shallow crustal earthquakes associated with regional fault systems [4]. Historical seismic data reveals that between 1990 and 2023, over 1,200 earthquakes of magnitude ≥4.0 occurred in the vicinity of the SNC [5] (Fig. 3a), with potential Peak Ground Acceleration (PGA) values reaching 0.6 g (588.399 gal) based on probabilistic seismic hazard maps [6]. The regional fault systems in West Java and Banten Province represent additional seismic risks beyond the subduction zone between the Eurasian and Indo-Australian plates (Fig. 3b) [4]. This seismic activity, combined with observed structural degradation, raises critical concerns about the facility's long-term resilience and operational safety. Damage to buildings from ground vibrations can be attributed to four key factors: local geological conditions, the interaction between the building structure and the ground, seismic properties, and the distance from the earthquake's epicenter [7].

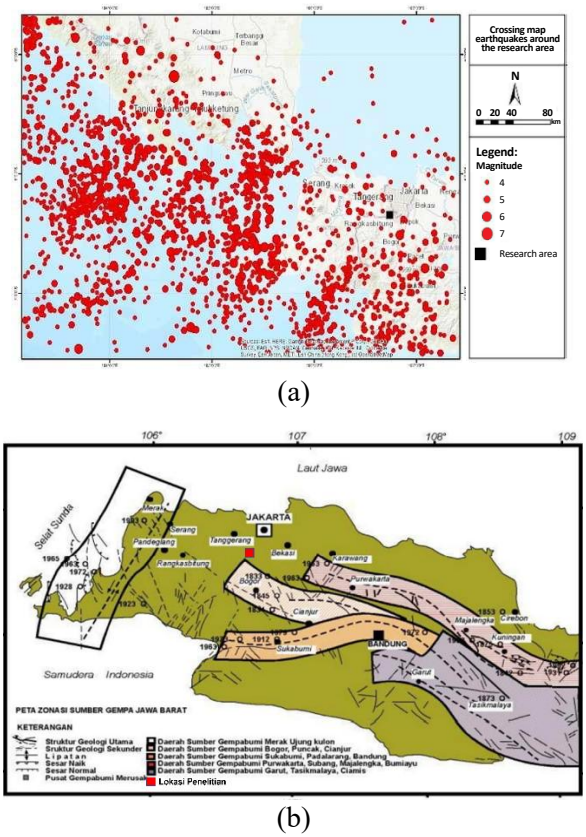

Fig. 3. (a) Earthquake distribution with ranging from M 4 to M 7 occurring around the SNC between January 1990 and January 2024, as documented in the United States Geological Survey (USGS) catalog [5], (b) Regional fault lines in West Java and Banten Province. These faults represent additional seismic risks beyond the subduction zone between the Eurasian and Indo-Australian plates [4].

International Atomic Energy Agency (IAEA) safety standards emphasize comprehensive site evaluation, including detailed seismic hazard assessments, to ensure reactor integrity under extreme events [8]. Current methodologies for assessing seismic vulnerability in nuclear facilities include microtremor-based techniques, which provide efficient and non-invasive approaches to characterizing both site conditions and structural response. The Horizontal-to-Vertical Spectral Ratio (HVSR) method has gained recognition for site characterization, as recommended by the Nuclear Energy Regulatory Agency (BAPETEN) for site studies [9]. The Floor Spectral Ratio (FSR) technique offers insights into building-specific dynamic behavior and vulnerability parameters [10,11]. Calculating fundamental frequencies is essential for understanding resonance phenomena, as the dynamic response of structures to earthquakes becomes critical when the frequency of ground movements approaches the structure's natural frequency [12]. IAEA, with the support of international experts, establishes and continuously updates safety requirements for the construction and operation of nuclear facilities, publishing standards that cover methodologies for determining seismic load assumptions, seismic design, and seismic safety for both new and existing nuclear facilities [13-16].

Despite the established importance of seismic safety assessment for nuclear facilities, comprehensive evaluation of the RSG-GAS complex using modern microtremor techniques remains limited. Previous studies have not adequately addressed the combined effects of aging-related structural degradation and seismic vulnerability in the context of Indonesia's unique tectonic environment. The microtremor method has proven effective for measuring dynamic characteristics of structures, as demonstrated in studies of the Leaning Tower of Pisa [17] and concrete structures [18,19]. However, the relationship between site-specific ground response characteristics and building-level structural performance requires detailed investigation to support evidence-based maintenance and safety enhancement strategies. The primary safety objective in the design, construction, and operation of nuclear facilities is to safeguard facility personnel, the public, and the environment from the harmful effects of ionizing radiation, requiring protection both during normal operations and in the event of accidents [20].

This study aims to provide a comprehensive seismic safety assessment of the RSG-GAS facility by integrating HVSR analysis for site characterization with FSR evaluation of structural vulnerability. The research objectives include:

(1) determining subsurface dynamic properties through dominant frequency, amplification factor, and seismic vulnerability indices; (2) evaluating building-specific parameters including resonance index, inter-level deviation, peak ground acceleration response, and building vulnerability indices; and (3) identifying critical zones requiring targeted structural reinforcement. This investigation will establish a framework for ongoing seismic safety monitoring and contribute to the development of risk mitigation strategies for nuclear facilities operating in seismically active regions. The study contributes to understanding seismic characteristics and structural resilience in the SNC, Indonesia's largest nuclear facility, providing crucial insights into ground stability and the facility's ability to withstand seismic forces under maximum potential ground acceleration conditions. This work contributes to the understanding of seismic characteristics and structural resilience in the SNC, Indonesia's largest nuclear power facility. It analyzes the subsurface properties through parameters such as dominant frequency (f_0), amplification factor (A_0), and seismic vulnerability (K_g), providing crucial insights into ground stability. Additionally, it examines the structural characteristics of the RSG-GAS reactor building under maximum potential ground acceleration, evaluating key parameters including resonance index (IR), inter-level gap (γ_j), the PGA of building structures (α_{bj}), and the building vulnerability index (K_{tgj}). These analyses enhance the assessment of earthquake impact and the facility's ability to withstand seismic forces.

METHODOLOGY

BAPETEN has recommended the use of microseismic methods for comprehensive site evaluation, particularly focusing on site characteristics and structure-soil interaction. This new analytical approach leverages microtremor observations to improve the estimations of ground motion characteristics. Specifically, the method analyzes the vertical and horizontal components of seismic waves. The spectral ratio of the Horizontal to Vertical Components (HVSR) is notably similar to the horizontal motion transfer function at the surface, as described by Nakamura (1989) [21]. The HVSR technique has become a widely adopted tool in microseismic data analysis, especially for assessing local effects and conducting microzonation studies. Its popularity stems from its simplicity and flexibility, as it enables direct estimation of resonance frequency without requiring detailed information about the shear wave velocity structure or underground geological conditions [22].

Several studies have utilized the HVSR method to estimate the soil's natural frequency and amplification factor. Additionally, other research has employed the FSR method to explore the relationship between the natural frequency of the soil and the resonance of buildings on different floors. By integrating these parameters, a comprehensive understanding of the current soil and structural conditions at the RSG-GAS reactor installation can be achieved. In this study, microtremor measurements were conducted at 20 locations within the SNC between January 8 and 19, 2023 (as shown in Fig. 4).

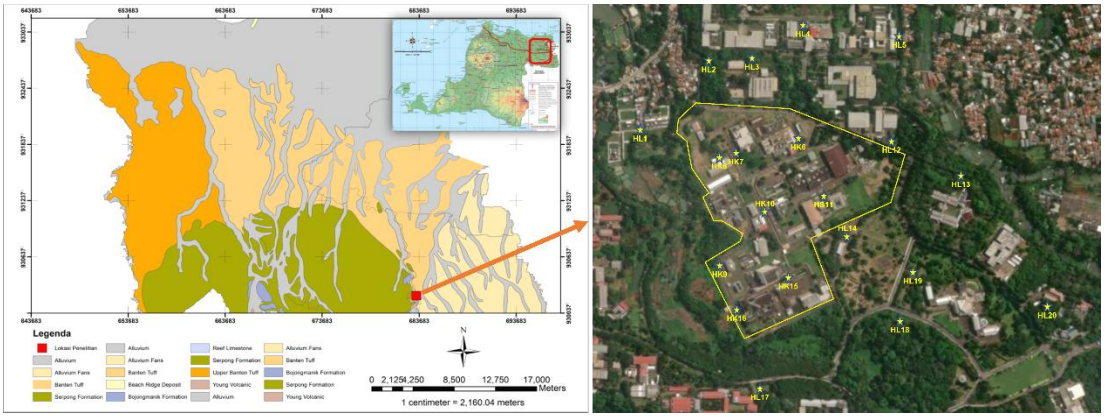

Fig. 4. Geological map of the SNC, located within Banten Province. The measurement location is marked with a red box. The location of the HVSR recording point are distributed throughout the SNC and surrounding areas, with a maximum distance of approximately 300 meters between each of the 20 measurement locations. The closest measurement point to reactor RSG-GAS are HK15 located approximately 30 meters away and HK9 located 124 meters away. The area outlined in yellow represents the SNC boundary. Recording point codes correspond to their positions: HK refers to points within the yellow boundary SNC, HS refers to points within the silver boundary, and HL indicates points outside the SNC.

FSR measurements were also carried out at the reactor and staircase buildings, covering a total of 31 locations (Figs. 5a-5e). The microtremors were recorded for 31 minutes at a sampling frequency of 100 Hz using the Lennartz Electronic LE-3D/20s seismometer (Fig. 5a). This device captures continuous analog signals in three components: two horizontal directions (NS, EW) and one vertical direction (Z), which are then digitized (Fig. 5b). For FSR processing, only the horizontal components are required. The data logging was performed using the DATAQ DI-710-ULS instrument, which is capable of recording, displaying, and storing data in real-time. The research workflow used to determine the characteristics of the RSG-GAS reactor and the staircase building is illustrated in Fig. 6. The key structural parameters identified in this study are summarized in Table 3.

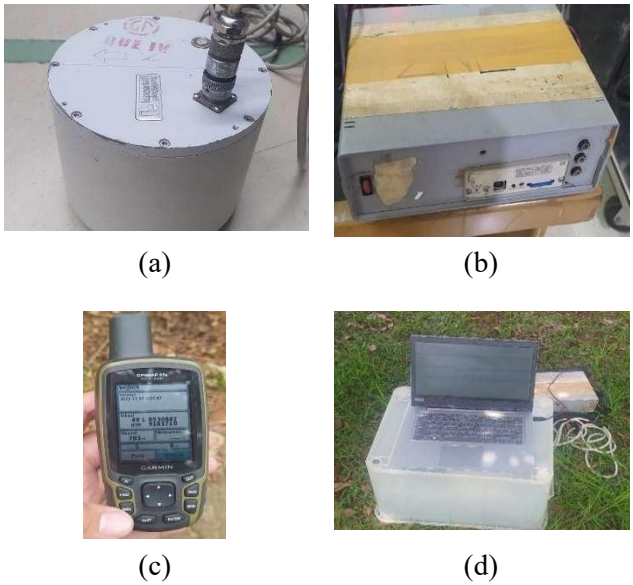

Fig. 5. The equipment used in this study includes: (a) a seismometer, (b) a data logger, (c) a handheld Global Positioning System (GPS) device, and (d) additional tools such as a container box, laptop, and specialized software for data recording and analysis.

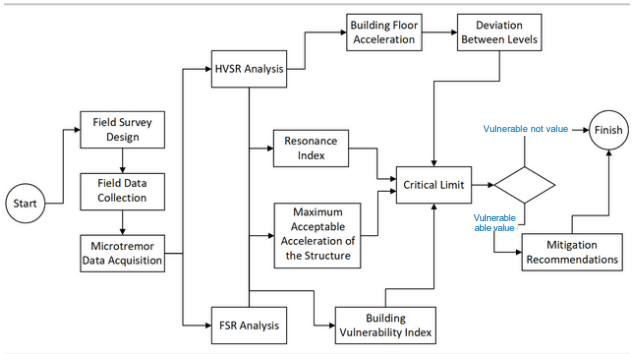

Fig. 6. Diagram of the research workflow used to determine the structural characteristics of reactor RSG-GAS installations, including both the reactor and staircase buildings.

Table 3. The result parameters of the FSR method provide a detailed characterization of the building structure, capturing key aspects of its dynamic behavior and response.

No	Research parameters	Critical limits	Actual value	Reference
1.	Resonance index	25 %	$I_R > 25$ %	[33]
2.	Inter-level gap	> 0.015 h_j	> 0.015 x (Tentative)	[36]
3.	PGA of building structures	> PGA (α_b)	> 558.97905 gal	[25]
4.	Building vulnerability index	$10^6 \frac{\gamma_{bj}}{\alpha_b}$	> 26.83464	[25]

In the processing phase, we began by calculating the soil's f_0 and A_0 using the HVSR method. Every object has a f_0 the specific rate at which it vibrates when subjected to external forces. This method monitors changes in physical properties by analyzing seismic ambient noise recorded at a single seismic station. To observe temporal variations in the natural resonance frequency, we employed the HVSR technique, as described by Khanmohammadi et al. (2021) [23]. Khanmohammadi et al. (2021) [23] approach explores the relationship between the natural period and the amplification factor at the study site, is based on the work of Konno & Ohmachi (1998) [24]. They proposed using peaks in the microtremor H/V ratio curve to determine natural period values, with logarithmically smoothed peak H/V ratios directly correlating with the amplification factor. Following this, we estimated the K_g for SNC and developed a seismic risk model for the site, guided by Nakamura et al. (2000) [25]. This model serves as a crucial reference for disaster mitigation, ensuring the safe and effective management of nuclear energy facilities while protecting the surrounding environment.

The seismic vulnerability value (K_g) represents the level of vulnerability of the surface soil layer to settlement during an earthquake. This index is closely related to geomorphological conditions, high index values are typically associated with soils composed of soft sedimentary rock lithology and indicating areas that are more vurnalable to dtrong ground shaking and potential damage in the event of an earthquake [27,28]. The seismic vulnerability value (K_g) can be found with the following Eq. (1) [28]:

$$K_g = \frac{{A_0}^2}{f_0} \quad (1)$$

Previous studies have extensively explored the relationship between earthquake - induced

damage and soil properties, with a focus on factors such as earthquake amplitude, frequency, and the dynamic behavior of buildings during and after seismic events [29-32]. These investigations have demonstrated that seismic energy transferred back to the ground from a vibrating structure can exacerbate building damage due to soil-structure resonance [32]. Researchers have examined ambient noise spectra in the NS and EW directions within buildings, analyzing the spectral ratios between the upper and lower floors, as well as conducting free-field measurements near the structures [18,34,35]. The FSR method, introduced by Herak (2011) [11], has become a standard approach for determining building transfer function parameters [18,34]. This method has been applied to study buildings, including 10-story structures with natural frequencies around 1 Hz, which are prone to resonance when subjected to vibrations at the same frequency. Resonance occurs when two objects share the same natural frequency; if one object (A) vibrates, the other object (B) will resonate and begin to vibrate in response. However, if a building's natural frequency differs from 1 Hz, its response to seismic events is likely to be smaller due to the absence of resonance [33].

Microtremor measurements were conducted at the Roman Colosseum by Nakamura et al. (2000) [25] to enhance its earthquake stability. The analysis revealed that the Colosseum's dynamic characteristics, including different natural frequencies and amplification factors for its inner and outer walls, were critical. The study proposed maximum acceptable acceleration values (α_{bj}) for various points in the Colosseum as a new seismic index, which was validated by correlating it with structural damage from the Apennines earthquake of 1349 [25]. For nuclear reactor building structures, safety objectives mandate strict adherence to protective measures, such as reactivity control, cooling of fuel elements, absorption of radioactive materials, and limiting radiation exposure. Components and structures essential for these functions are considered safety-related [35]. The resonance index value aims to identify potential resonance risks that may occur in the building structure in the event of an earthquake event around the building. It is calculated by Eq. (2):

$$IR = \left|\frac{f_b - f_g}{f_g}\right| x100\ \% \tag{2}$$

where, IR is building resonance index, f_b is natural frequency building, and f_g is natural frequency of ground.

The deviation between the levels is the difference between the horizontal deviation of the floor structure and the previous floor and then compared with the difference in floor levels according to the equation. Structural deformation is not only concerned with the dynamic properties of layers and surface structures. but also with subsurface seismic movements. Understanding soil and structural resilience is important for assessing potential damage from future earthquakes. The transfer of energy or seismic movement within a structure horizontally relates to the mass of the rock and the dynamic properties of the ground surface and its structure. Spectral amplification of soil movement occurs when the structural load response differs from the soil movement response, i.e. the ratio of mass to soil motion. Amplification affects the horizontal deviation of the structure [25]. The equation of horizontal deviation of a structure can be written as follows Eq. (3).

$$\delta_j = \frac{\alpha_{sj}}{(2\pi f_b)^2} \tag{3}$$

While α_{sj} is the floor acceleration value obtained based on the formula Eqs. (4,5) [25]:

$$\alpha_{sj} = A_g \,.A_{sj}.\alpha_b \tag{4}$$

$$A_{sj} = \frac{S_{H\ Building}}{S_{H\ Ground}} \tag{5}$$

SNI 1726:2019 regulates the limit of the permissible inter-level deviation value for Risk Category IV buildings must not exceed 0.015 times the floor level (h_j). So the allowable deviation between levels is 0.015 multiplied by the height of the floor (h_j) [36]. On the structure of a multi-storey building. The equation will be influenced by the different height levels of the existing building structure. So that the equation can be changed to get the value of the deviation between levels as follows Eq. (6) [25].

$$\gamma_j = \frac{\delta_j - \delta_{j-1}}{h_j} = \frac{\alpha_{sj} - \alpha_{sj-1}}{4\pi^2 {f_b}^2 h_j} \tag{6}$$

If unit γ_j is 10^{-6}, h_j is meter and seismic acceleration is measured in unit Gal (cm/s^2), than with the unit adjustment, Eq. (7) can be written in following form Nakamura et al., (2000) Eq. (7) [25],

$$\gamma_j = \frac{10^4\left(A_{sgj} - A_{sgj-1}\right)}{4\pi^2 {f_b}^2 h_j}\alpha_b \tag{7}$$

PGA is the value of the maximum potential change in soil speed owned by a site location by studying the history of earthquakes that occur around the site location and the potential for earthquakes caused by various existing earthquake sources. The PGA value is a reference as the maximum PGA value for reactor building structures and staircase buildings (critical limit values) [6] in determining α_{bj} at each FSR recording point. The following is the result of the analysis of the value of the acceleration value that can happen in the building structure α_{bj} at each point of the FSR based on the following Eq. (8) [25].

$$\alpha_{bj} = \frac{10^4 4\pi^2 {f_b}^2 h_j}{A_{sgj} - A_{sgj-1}} \gamma_{bj} \quad (8)$$

Note: α_{bj} in gal units

The amplification of the structure to the soil (A_{sgj}) is a comparison of the horizontal spectrum of the building on each floor with the NS component and the EW component compared to the vertical spectrum of the soil. The vulnerability of a building can be quantified to show how strong and weak a building is in the face of earthquakes. For this reason, Nakamura et al. (2000) triggered the Building Vulnerability Index (K_{tgj}) in units of 1/gal through Eq. (9) [25].

$$K_{tgj} = \frac{10^4 \left(A_{sgj} - A_{sgj-1}\right)}{4\pi^2 {f_b}^2 h_j} \quad (9)$$

from Eqs. (8) and (9), the critical limit value for the building vulnerability index in the Eq. (10),

$$10^6 \frac{\gamma_{bj}}{\alpha_b} \quad (10)$$

The structural vulnerability index estimated using function parameters is used to identify building vulnerability [26,37].

RESULTS AND DISCUSSION

Horizontal to Vertical Spectral Ratio (HVSR)

Following the collection of microseismic data, a reliability test was conducted to assess the acceptance of peak curve values. The reliability test indicated that only 8 measurement points satisfied the acceptance criteria, while 12 measurement points failed to meet the required standards and were therefore excluded from subsequent data processing stages [38]. The poor data quality at these excluded points can be attributed to various environmental and subsurface conditions at the measurement locations. Figure 7 shows that the f_0 values for points HL3 and HK10 differed significantly from the other measurement points. While the remaining points demonstrated an average f_0 value of approximately 3 Hz, HL3 and HK10 exhibited multiple peaks, with some peaks aligning closely with the average f_0 value observed in the SNC area and its surroundings. This discrepancy is likely attributable to the presence of very soft sediment at these specific points (Table 4), which resulted in a more dominant f_0 value compared to the regional average in the SNC area. The analysis revealed that HL3 had an estimated f_0 of 3.832 Hz, with A_0 at 2.268 and K_g at 1.343. Similarly, HK10 demonstrated an f_0 of 4.436 Hz, with A_0 at 2.245 and K_g at 1.136. Consequently, the f_0 value for the SNC region ranged from 2.846 Hz to 4.436 Hz, with an average f_0 of 3.496 Hz [39]. These results indicate a generally homogeneous soil layer throughout the B. J. Habibie KST area. Table 5 and Fig. 8 summarize the results obtained from the eight reliable recording points.

Given that the distances between these measurement points complienced with established guidelines [38], these points adequately represent the research location within the SNC area, where nuclear energy facilities, including the RSG-GAS reactor, are situated. Therefore, additional measurements at other recording points were deemed unnecessary. The findings align with previous research by Al-Amri et al. (2022), who measured HVSR ratios to map seismic vulnerability indices [7]. Through microtremor measurements at over 260 locations, they developed comprehensive maps displaying fundamental resonance frequencies and maximum relative amplification. These results provided valuable insights for civil engineers and urban planners by identifying areas with heightened susceptibility to seismic activity, thereby enabling improvements in building construction practices and updates to building codes to enhance safety and resilience against earthquakes.

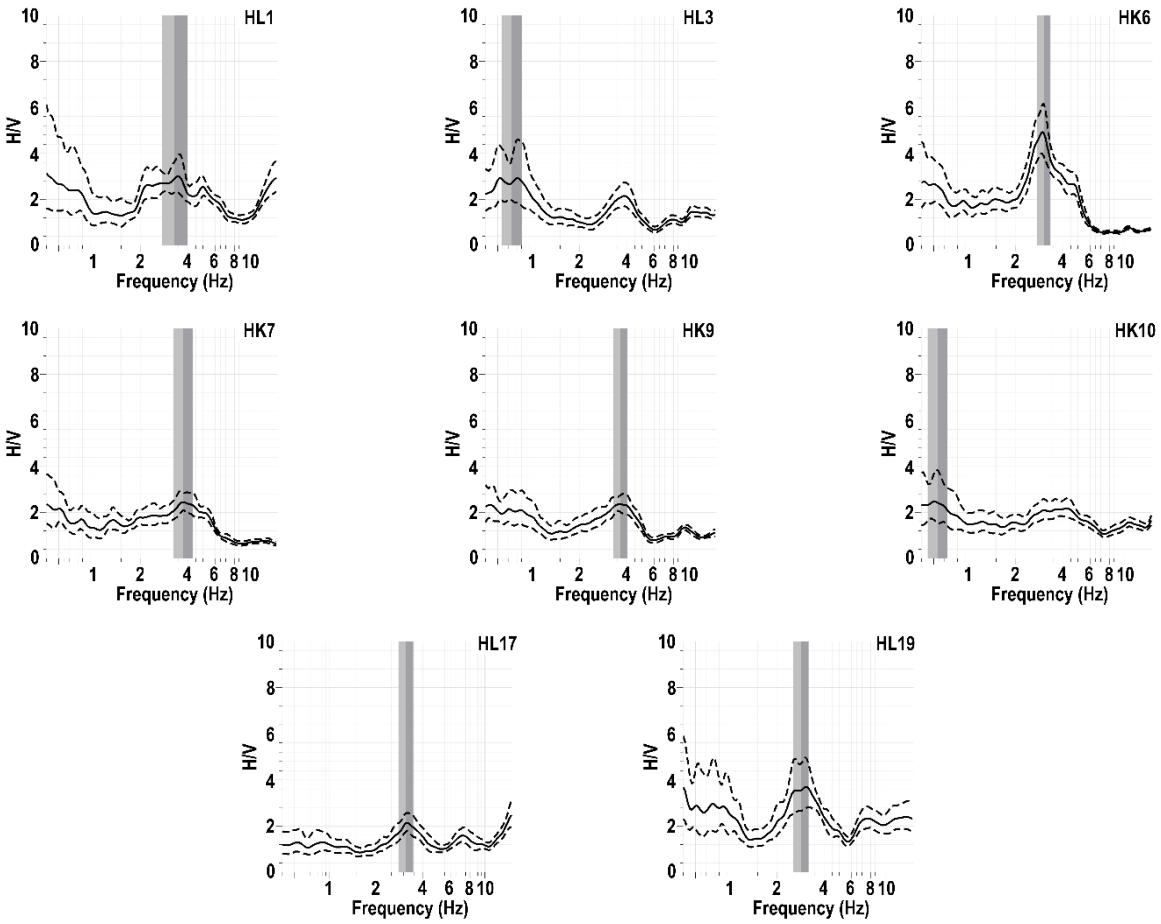

Fig. 7. The HVSR curve for the SNC ware generated eight acceptable recording points out of twenty recorded. The HK9 point is a measurement point that is a reference for measuring the characteristics of the reactor building because it has the closest distance from the reactor building with a distance of 124 meters.

Table 4. Soil classification is determined based on the natural frequency of microtremors, following the criteria established by Kanai and Omote-Nakajima modified from [40].

Soil classification			Frequency / f_0 (Hz)	Kanai classification	Description	Character
Type	type/ kanai	Omete-Nakajima				
IV	I	A	6.67 - 20	Tertiary rocks are older. Composed of hard sandy gravel rocks, etc.	The thickness of the surface sediment is very thin, dominated by hard rocks	Hard
	II		4 - 10	Aluvial rock with a thickness of 5 meters, consisting of sandy - gravel, dandy hard clay, loam etc.	The thickness of surface sediment belongs to the intermediate category of 5-10 meters	
III	III	B	2.5 - 4	Alcove rock, with a thickness of > 5 meters. Composed of sandy-gravel, sandy hard clay, loam, etc	The thickness of the surface sediment belongs to the thick category of about 10-30 meters	Soft
II	IV	C	<2.5	Alluvial rocks formed from delta sedimentation, top soil, mud, etc. with a depth of 30 meters or more	The thickness of the surface sediment is very thick	Very Soft

Table 5. Results of HVSR data processing and seismic vulnerability index for SNC and surrounding areas.

Mesurenment point	Coordinates			f_0	A_0	Kg
	Degree		Elevates			
	Latitude	Longitude	M	Hz		
HL1	-6.348272	106.659758	39	3.3014	2.8934	2.5358
HL3	-6.346490	106.662627	58	3.8321	2.2687	1.3431
HK6	-6.348583	106.663896	59	3.0277	4.8886	7.8932
HK7	-6.348927	106.662213	56	3.7645	2.4339	1.5736
HK9	-6.351719	106.661803	52	3.6544	2.3433	1.5026
HK10	-6.350566	106.663061	55	4.4362	2.2454	1.1365
HL17	-6.355076	106.662416	53	3.1082	2.1149	1.4391
HL19	-6.352133	106.666715	60	2.8468	3.5366	4.3936

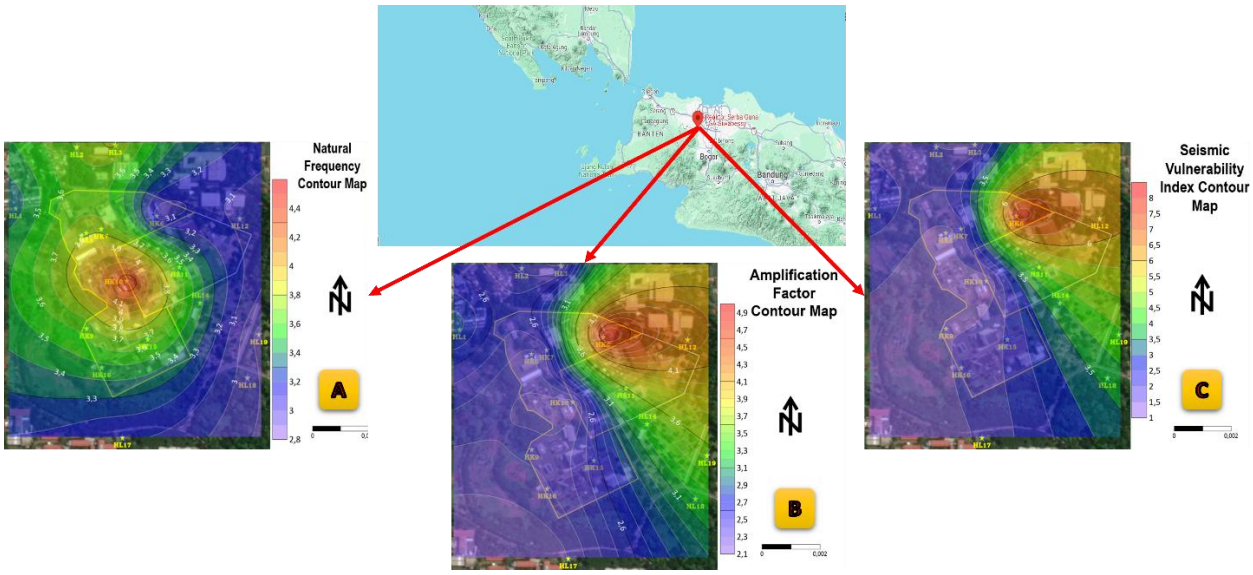

Fig. 8. The results of this study are presented as contour maps derived from the HVSR data processing for the SNC within the KST B. J. Habibie. This data collection aims to provide an up-to-date representation of the subsurface conditions in the SNC, home to Indonesia's largest array of nuclear power installations, including the RSG-GAS reactor. The findings are depicted in three contour maps: (a) the natural frequency contour map, (b) the amplification factor contour map, and (c) the seismic vulnerability index contour map.

Floor Spectral Ratio (FSR)

Figure 9 presents the results of the FSR analysis, displaying wave spectra processing curves for both NS and EW directions. The analysis revealed several non-ideal conditions, primarily characterized by curves that lacked clear peak values in the spectrum amplitude. These suboptimal conditions arose mainly from the inability to maintain a silent measurement environment due to continuous operational vibrations generated by essential safety systems of the nuclear reactor. The persistent vibrations originated from multiple reactor safety systems that were operated continuously, even during reactor shutdown periods. These systems include the air ventilation system, radiation protection system, reactor water circulation system, reactor protection system, and various electrical systems. Furthermore, variations in floor area, elevation levels, and internal geometries within the reactor building contributed to the non-ideal measurement conditions. The reactor building incorporates several thick steel sheets embedded in concrete for safety protection, which potentially introduced additional vibrational interference. These environmental factors likely influenced the accuracy of other parameter analyses conducted in this study. Despite these methodological limitations, the study provided valuable insights into the structural characteristics of both the reactor building and the staircase building, thereby supporting ongoing reactor management efforts.

A comparative analysis was conducted to examine the amplitude patterns (power spectral density) between the reactor building (Figs. 9a-9d) and the staircase building (Fig. 9e). The analysis revealed distinct differences in amplitude distribution between the two structures. The staircase building demonstrated a more coherent pattern, characterized by a gradual and consistent increase in amplitude from the lowest to the highest levels. Conversely, the reactor building exhibited less uniformity in amplitude values across different elevations. These observed differences can be attributed to several structural and operational factors. The reactor building's irregular amplitude pattern resulted from the predominant activities of reactor support systems, which generated higher operational vibrations throughout the structure. Additionally, the heterogeneous layout of the reactor building across various levels contributed to the non-uniform amplitude distribution. In contrast, the staircase building operated with fewer active support systems and maintained a more homogeneous architectural layout, resulting in a more predictable amplitude increase with elevation. The findings suggest that building height correlated with seismic vibration amplification. Structures at greater elevations were more susceptible to amplified vibrations during seismic events, while lower floors experienced reduced vibrational impact, consequently producing lower amplitude values. This height-dependent amplification pattern would has significant implications for seismic risk assessment and structural design considerations in multi-level nuclear facilities.

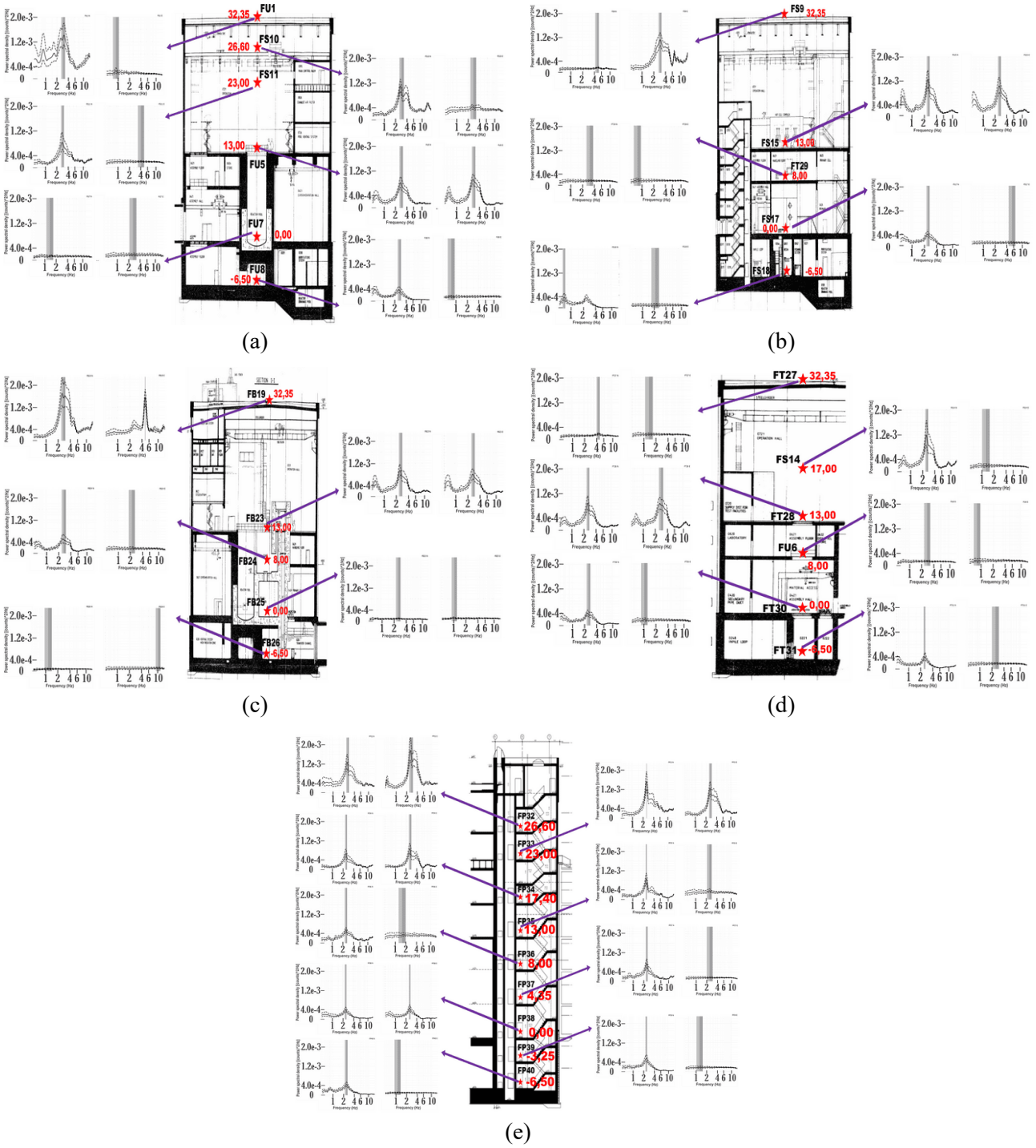

Fig. 9. Spectra measurement of NS (right panel) and EW (left panel) components for the reactor and staircase building. The distribution is determined based on the placement of the measurement point and has the same location on each floor based on the distance to the outermost reactor RSG-GAS building wall. (a) Reactor building, north side, (b) reactor building, south side, (c) reactor building, west side, (d) reactor building, east side, (e) staircase building.

The response of a building is significantly influenced by its natural frequency, which refers to the number of vibrations the building undergoes per second. Each building has a unique natural frequency, largely determined by its height. Taller buildings tend to vibrate more slowly than shorter ones. The results indicated that when the frequency of ground vibrations was lower than a building's natural frequency, the building experienced less damage from deformation. However, the findings showed that as the frequency of ground vibrations approached the building's natural frequency, the likelihood of deformation increased. The analysis revealed that when the ground vibration frequency matched the building's natural frequency, resonance occurred, which led to maximum deformation and a heightened risk of structural damage [41].

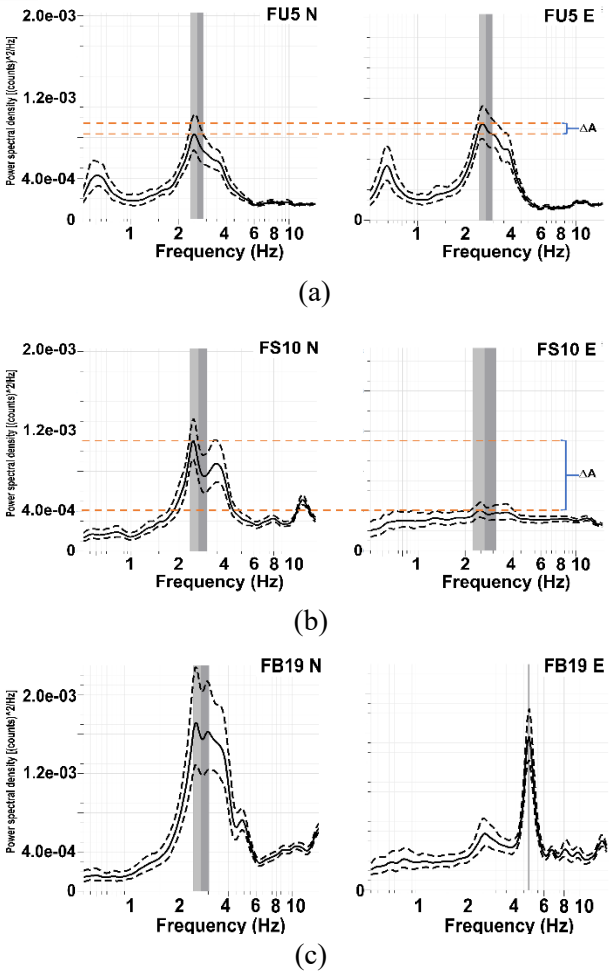

Fig. 10. FSR spectrum analysis result curve for microseismic recording of reactor building north side depicting f_0 and A_0 values from both directions of NS (left) and EW (right) wave components. (a) Recording point FU5 was located at an elevation of 13 meters, (b) Recording point FS10 is located at level 26.60 meters, (c) Recording point FB19 is located at level 32.35 meters.

Figure 9 shows several anomalies that were obtained from the analysis of the FSR spectrum curve recordings in the RSG-GAS reactor building and the staircase building. A good curve for FSR recording is generally depicted in Fig. 10a, which demonstrates the criteria of having amplitude and frequency values that show minimal differences between the NS and EW components. The analysis revealed that the anomaly described by the Fig. 10b curve exhibited a significant difference in amplitude value, while the Fig. 10c curve, although it showed a small difference in amplitude, demonstrated a significant difference in frequency value. The results indicated that this anomaly was likely caused by noise originating from the SSK, which remained operational to support the safety of the RSG-GAS reactor. The findings showed that the noise occurred due to the dominance of the wave direction in certain components, manifesting as variations in frequency or amplitude values. The analysis further revealed that another factor affecting the frequency and amplitude values obtained in Fig. 9 was the elastic modulus parameter of the building structure around the FSR recording point [42]. The investigation confirmed that some parts of the reactor building structure possess special features in the form of steel plate coating designed to protect the reactor facilities and other nuclear materials from external security attacks [43].

Resonance Index (IR)

The Resonance Index (IR) was assessed by comparing the natural frequency of the reactor RSG-GAS installation site with the natural frequencies measured at various points within the building structure, as obtained from FSR spectrum data processing. Table 5 shows that the natural frequency value for the reactor building site was represented by the HK9 point, as it is located closest to the reactor RSG-GAS installation. Figure 11 presents the analysis results, which details the potential resonance index values at each measurement point for both the reactor building and the staircase building. The investigation revealed that due to the non-ideal conditions of microseismic recordings, which could not be conducted in a completely silent environment, external disturbances affected the data quality. The analysis indicated that despite efforts to minimize these disturbances, anomalies in the results occurred. Figure 11 demonstrates that the resonance potential at each measurement point is illustrated by the calculated resonance index values, providing a comprehensive assessment of structural vulnerability to resonance effects.

Fig. 11. One of the measurement points for the south side of the reactor building (point FS9). In the northern part of the reactor building, there is an air ventilation chiller system that operates continuesly throughout a day to ensure the air quality in the reactor building is consistently maintained. The green solid circle above the ventilation system chiller shows the chiller that was operating at the time the recording was taken.

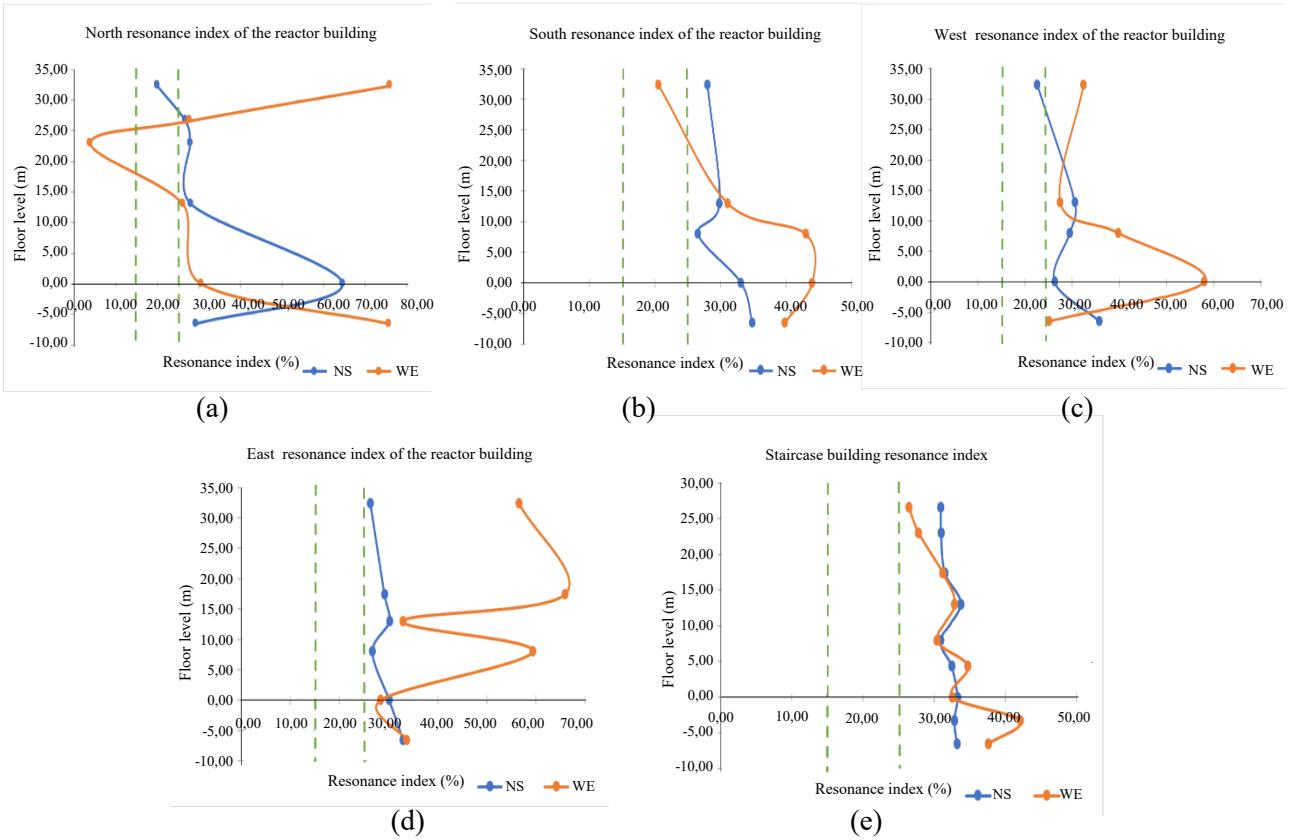

Fig. 12. Graphic distribution of resonance index at each measurement point in the building based on floor height. The blue graph line represents the distribution of the NS direction wave spectrum and the orange graph represents the WE direction wave spectrum distribution. The vertical green line on the left is the lower limit value (15 %), and the vertical green line on the right is the upper limit value (25 %) as the critical limit value. These two value limits divide them into three assessment categories (high, medium and low). (a) Reactor building, north side, (b) reactor building, south side, (c) reactor building, west side, (d) reactor building, east side, (e) staircase building.

Fig. 13. Cracks found during visual inspection in 2019 in the area adjacent to point FS11. (a) areas of cracks in the floor structure, (b) cracks in the wall structure and some cracks have been repaired with concrete injection [3].

The results showed that the majority of measurement points were positioned to the right of the second green line, indicating that most points in the reactor building and all points in the staircase building demonstrated an *IR* value above 25 %, which reflects a low likelihood of resonance [33]. Figures 12a-12c present three measurement points with *IR* values between 15 % and 25 %, specifically ranging from 20.07 % to 22.63 %. The analysis revealed that these points suggested a moderate potential for resonant events, with all three points located at the same height of 32.35 meters (roof level). The investigation indicated that the elevated *IR* values at this level were attributed to the presence of a ventilation system, including a chiller pump situated on the north side of the reactor building, which was operated continuously to provide clean air (Fig. 11). Figure 12a shows a measurement point with an *IR* below the critical value of 15 %, specifically at 3.98 % at a height of 23 meters. The results indicated that this low *IR* value suggested a high potential for resonance, as it approached 0 %, demonstrating that the natural frequency at this point was near that of the building's fundamental frequency (HK9 measurement point). The analysis revealed that the high *IR* value at this location (FS11) was likely due to its proximity to a hallway adjacent to the reactor protection system room. The findings showed that the reactor protection system, an electrical cabinet that continuously emits vibrations, contributed to the building structure's vibrational response. The investigation confirmed that this system was designed with earthquake-resistant specifications to minimize damage risk during seismic events. The analysis further indicated that this measurement location was also positioned close to the location where structural damage occurred in 2019 (Fig. 13) [3].

Figure 12 shows the obtained *IR* anomalies across different measurement levels. The analysis revealed significant differences in *IR* anomalies (exceeding 5.00 %) between the NS and EW wave components at multiple floor levels: 32.25 meters (Figs. 12a-12d), 23.00 meters (Fig. 12a), 17.40 meters (Fig. 12d), 8.00 meters (Figs. 12b-12d), 0 meters (Figs. 12a-12c), -3.25 meters (Fig. 12e), and -6.50 meters (Figs. 12a and c). The results indicated that the difference values ranged from 7.45 % to 55.96 %. The investigation suggested that the possible cause originated from vibrations produced by the reactor support system, which remained operational around the recording points. The findings showed that this operational system provided vibrational input with dominant directional components between NS and EW orientations to the seismometer measuring instrument, resulting in the observed directional bias in the recorded data.

Inter-level deviation (γ_j)

The results of this study showed that the inter-level deviations at all measurement points were very small and remained below their respective critical limit values. Table 6 demonstrates that the variation in critical limit values across different sides of the reactor building was attributed to the structural differences at each side and height level. The analysis indicated that this diversity of critical limit values served as an essential reference for safety assessments and analysis in this research. The findings revealed that all measurement points recorded values of less than 0.5 cm. The investigation suggested that this outcome was likely due to the reactor building's robust design, which was engineered to withstand seismic shocks, one of the key disaster risks in nuclear reactor installations. The analysis confirmed that the design and planning of reactor buildings adhered to well-established international regulations, such as those set forth by the IAEA, ensuring structural integrity and safety under various loading conditions.

PGA of building structures (α_{bj})

The PGA value serves as a critical threshold to assess the structural characteristics of the reactor building. The analysis indicated that if the recorded acceleration value dropped below the PGA threshold, it would indicate potential structural damage at the corresponding measurement point, since the building might not be able to withstand the acceleration if it reached the critical limit value. Conversely, the results showed that when the acceleration value of the structure exceeded the critical limit, it indicated that the structural integrity of the building could withstand up to the recorded acceleration value (passing the critical limit value). Figure 14 presents the analysis of the potential acceleration values for the building structure α_{bj} at each FSR measurement point. The investigation revealed that the structural integrity of the reactor and staircase building could be considered safe if the acceleration value exceeded the specified critical threshold. The analysis confirmed that Peak Ground Acceleration (PGA) can be determined using empirical formulas, either based on historical records of major earthquakes in the area or by assessing the likelihood of future seismic events using existing geological risk data.

Table 6. The deviation value between the levels obtained on the reactor building structure on each side of the building with the staircase building structure. The table is also equipped with the critical value of each measurement point which varies depending on the height of each floor on each side of the reactor building, this is indicated by several levels that do not have a value at a certain level.

Level (meter)	Reactor building												Staircase building		
	North			South			West			East					
	Critical limit	NS	EW	Critical limit	NS	EW	Critical limit	NS	EW	Critical limit	NS	EW	Critical limit	NS	EW
32.35	8.625	0.027	0.091	29.025	0.010	0.006	29.025	0.005	0.005	22.425	0.006	0.008	-	-	-
26.60	5.400	0.002	0.016	-	-	-	-	-	-	-	-	-	5.400	0.025	0.017
23.00	15.000	0.006	0.009	-	-	-	-	-	-	-	-	-	8.400	0.003	0.001
17.40	-	-	-	-	-	-	-	-	-	6.600	0.001	0.030	6.600	0.007	0.015
13.00	19.500	0.005	0.005	7.500	0.032	0.016	7.500	0.014	0.011	7.500	0.010	0.010	7.500	0.001	0.002
8.00	-	-	-	12.000	0.004	0.009	12.000	0.006	0.008	12.000	0.003	0.013	5.475	0.005	0.012
4.35	-	-	-	-	-	-	-	-	-	-	-	-	6.525	0.002	0.003
0.00	9.750	0.011	0.038	9.750	0.008	0.006	9.750	0.000	0.018	9.750	0.001	0.001	4.875	0.003	0.000
−3.25	-	-	-	-	-	-	-	-	-	-	-	-	4.875	0.008	0.011
−6.50	-	-	-	-	-	-	-	-	-	-	-	-	-	-	-

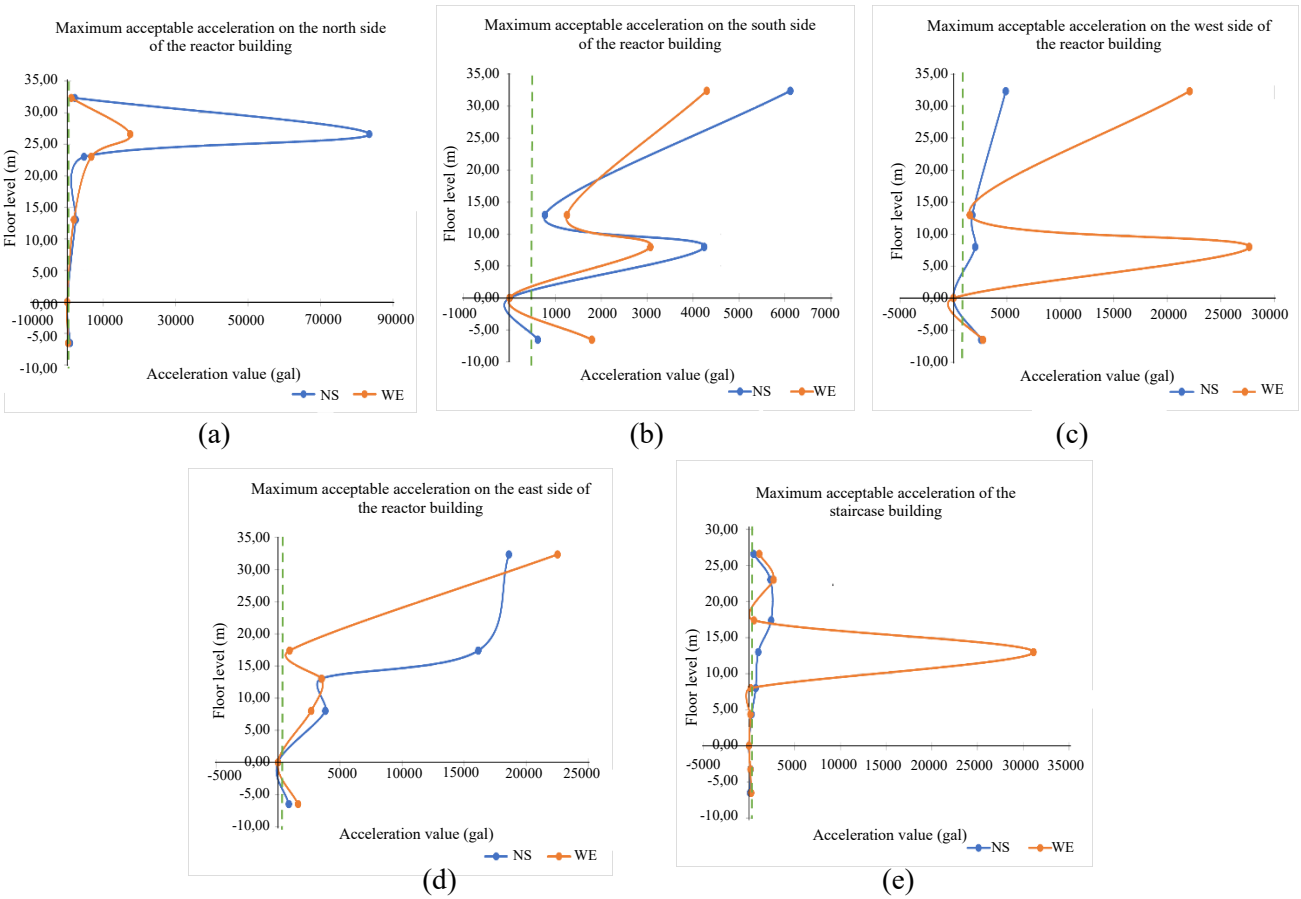

Fig. 14. The graph distribution of the maximum acceleration value that can be received by the building structure from the measurement point located at each floor level in the building (reactor building and staircase building) based on the results of the analysis. The blue graph line represents the spectral distribution of the NS directional wave. The orange represents the distribution of the WE directional wave spectrum. and a dotted green line as a safety limit value based on previous research references. (a) Reactor building, north side, (b) Reactor building, south side, (c) Reactor building, west side, (d) Reactor building, east side, (e) Staircase building.

Figure 14 shows acceleration anomalies with significant differences (exceeding 2000 gal) between the NS and EW wave components at multiple floor levels: 32.25 meters (Figs. 14c-14d), 26.60 meters (Fig. 14a), 17.40 meters (Fig. 14d), 13 meters (Fig. 14e), and 8 meters (Fig. 14c). The results indicated that the difference values ranged from 3,918.439 gal to 66,018.893 gal. The findings showed that this pattern was consistent with the results obtained for the *IR* anomaly values and was most likely caused by the same factor: the reactor support system remained operational during the microseismic recording process. The analysis revealed that this similarity arose from the relationship between Eq. (7) and its parameters, which were derived from Eq. (5). The investigation showed that Eq. (5) represented a comparison between the horizontal spectrum of the building and the horizontal spectrum of the ground. The results indicated that the horizontal spectrum was obtained from seismometer recordings, which integrated the acceleration and frequency values measured along the NS and EW components.

The analysis of the acceleration graph revealed that the significant difference in values between the NS and EW components at certain points complicated the interpretation of the results. Figure 14a shows a pronounced anomaly at the 27-meters level, where the investigation indicated that the difference between the two components was very large. Figure 10b demonstrates that the acceleration anomaly observed in Fig. 14a originated from the difference in the frequency values of the NS and EW components in the spectrum curve analysis. The results suggested that the significant variation in spectrum curve values was likely due to the influence of noise waves that were detected during the microseismic recording at point FS10 (Fig. 14a). The findings indicated that this noise interference contributed to the directional bias observed between the horizontal components, resulting in the substantial discrepancies in the recorded acceleration values.

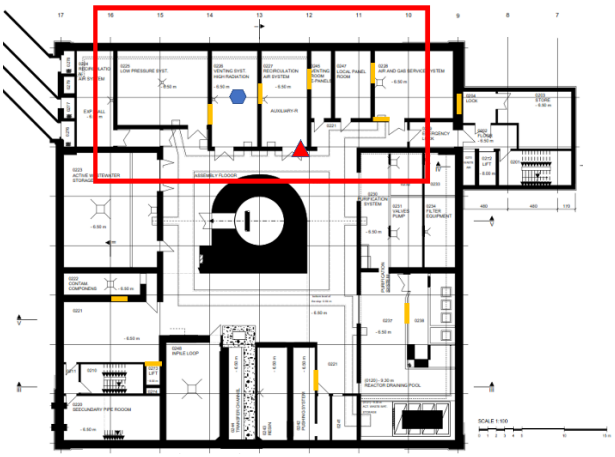

(a)

(b)

(c)

(d)

Fig. 15. Structural damage apparent on visual inspection in 2019 at floor -6.5 meters. (a) Location of damage to the floor structure -6.5 meters, the yellow dot is damage to the wall structure, the blue is damage to the floor structure, and the red is damage to the concrete structure. The area marked with a red box is structural damage close to point FU8. (b) Structural cracks on the adjacent floor at point FU8, (c) and (d) Structural cracks in the adjacent walls at point FU8, and this damage has been repaired with concrete injection [3].

Based on the results shown in Fig. 14 and the analysis presented in Fig. 10, acceleration values exhibiting significant differences between the NS and EW components were excluded from the conclusions of this study. Figure 14 illustrates the acceleration values recorded at various points in the reactor and staircase buildings. The analysis revealed that the acceleration values exceeded the critical threshold at all recording points, except for the point at 0 meters (not included) and point FU8. The results showed that the acceleration values for the RSG-GAS reactor building ranged between 617.684 gal and 4,673.450 gal for the NS wave component, and between 272.630 gal and 6,647.347 gal for the EW wave component. The investigation indicated that the lowest acceleration value, below the critical limit, was observed at FU8, where a measurement of 272.630 gal was recorded in the EW direction at a height of -6.5 meters on the north side of the RSG-GAS building. The findings showed that this area was primarily occupied by electrical cabinets, which minimized potential disturbance from wave noise. The analysis revealed that the characteristic PGA values at FU8 were below the critical limits established for this study area, indicating that further research was needed to validate these observations. The results suggested that structural engineering interventions might be required to strengthen the integrity of buildings in the FU8 area.

Figure 15a demonstrates that the FU8 recording location was positioned close to some damage identified in the 2019 inspection report, particularly on the north side of the reactor building. Table 2 shows that the reported damages consisted of five damages to the wall structure (Figs. 15c-15d), one report of damage to the floor structure (Fig. 15b), and one damage to the concrete structure (Fig. 2c) [3]. The investigation confirmed that these correlations between low acceleration thresholds and existing structural damage reinforced the need for further studies to validate these values. The analysis indicated that technical measures were required to strengthen building structures in the FU8 area to ensure continued structural integrity.

Based on the information obtained, the investigation suggested that the damage data recorded in 2019 most likely represented damage that occurred due to the accumulation of initial impacts resulting from the construction of reactor support facilities, which were built in 1993 and located around the reactor building. The analysis indicated that this was because the construction process used "Earth Nail" technology, which caused wave propagation (ground acceleration) in the reactor building area to increase in intensity during

the construction process. The findings showed that since that year, there had been gradual weakening at several structural points, which was consistent with the conditions documented in the 2019 report (Pujiarta et al., 2019) [3]. For the staircase building, the results indicated that acceleration values ranged from 969.0254 gal to 24,174.260 gal for the NS wave component and from 1,527.452 gal to 27,087.503 gal for the EW wave component. The analysis revealed that these values indicated that, relative to the maximum PGA potential and critical limit of this study, all recording points on the stairwell exceeded the critical limit value of 588.399 gal or 0.6 g. The investigation confirmed that this performance demonstrated the structural robustness of the staircase building under the current seismic conditions.

Building vulnerability index (K_{tgj})

The vulnerability of a building can be quantified to evaluate its resilience to earthquakes. The analysis revealed that the vulnerability index ranged from 1.328 to 50.689 for the NS wave component and from 0.230 to 74.628 for the EW wave component, with a critical limit set at 26.834. Figure 16 shows that several measurement points exceeded this critical limit. The results indicated that for the NS component, the vulnerability index ranged from 40.272 to 50.689 at points FU1 and FU7 on the north side of the reactor building and FS15 on the south side. For the EW component, the investigation showed that the vulnerability index ranged from 31.107 to 74.628 at points FU1 and FU8 on the north side, FS15 on the south side, and FS14 on the east side of the reactor building.

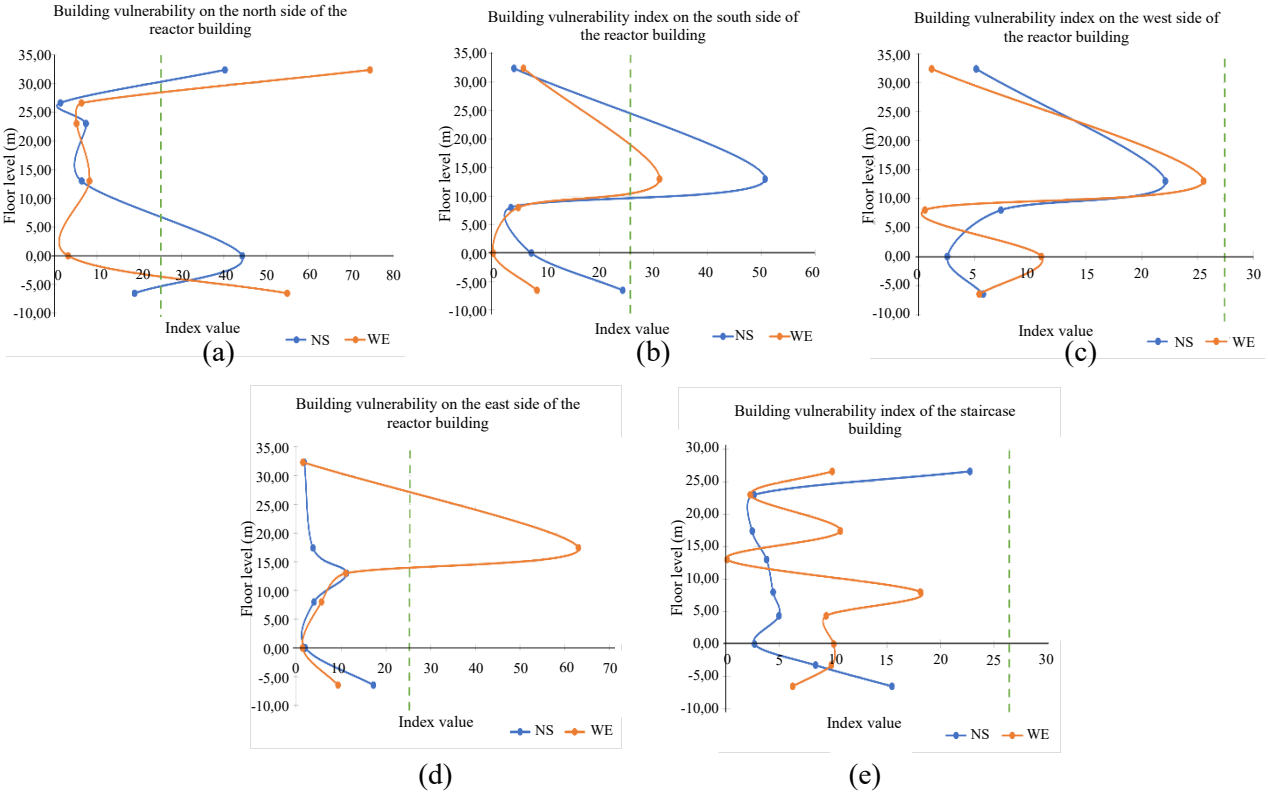

Fig. 16. The graph distribution of the value of the building structure vulnerability index from the measurement points located at each floor level in the building (reactor building and staircase building) based on the results of the analysis. The blue graph line represents the spectral distribution of the NS directional wave. The orange color represents the distribution of the WE directional wave spectrum. and a dotted green line as the critical boundary value. (a) Reactor building, north side, (b) reactor building, south side, (c) reactor building, west side, (d) reactor building, east side, (e) staircase building.

The findings suggested that these anomalies were likely due to noise from the reactor's supporting systems, which were running during the microseismic recordings and influenced the results. The analysis indicated that applying public building standards, such as SNI 1726:2019, to reactor buildings was problematic since reactor structures were designed to withstand a variety of potential external impacts over extended periods. The investigation revealed that the current analysis provided an overview of the building vulnerability index, demonstrating that continuous vibrations from the reactor's operational systems affected the building's vulnerability assessment. The 2019 visual

inspection report documented building structure vulnerability at recording locations that exceeded the critical limit in the reactor building. Figure 16a shows that for the north side of the reactor building, conditions at the -6.5 meters level (point FU8) were depicted in Fig. 15, while Fig. 17 illustrates that for the 0.0 meters level condition (point FU7), cracks were observed in 2019. The results showed that for the staircase buildings, all recording point values fell below their critical limits, ranging from 2.453 to 22.742 for the NS wave component and from 0.125 to 18.138 for the EW wave component. The analysis confirmed that this performance indicated superior structural integrity of the staircase building compared to specific vulnerable areas in the reactor building.

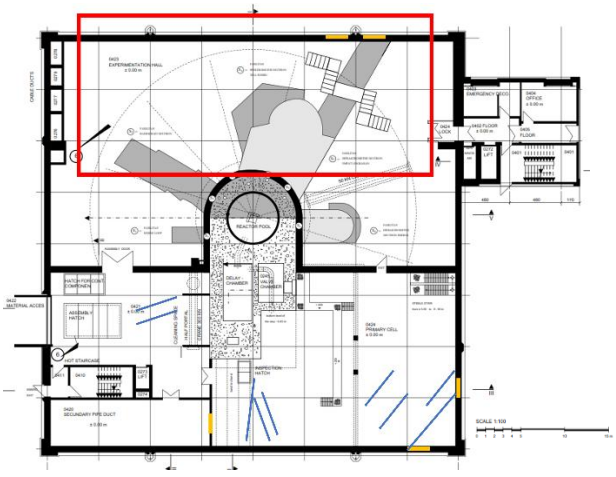

(a)

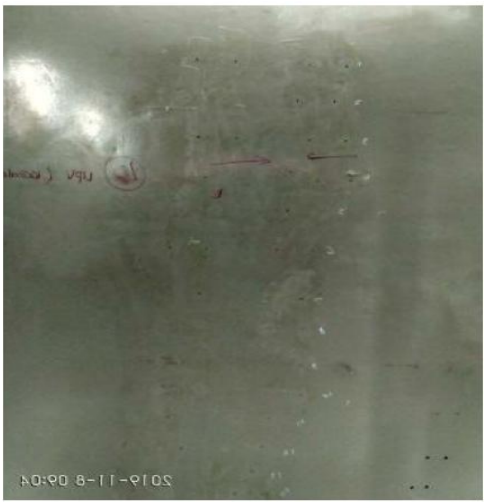

(b)

Fig. 17. Damage occurred during visual inspection in 2019 in the area adjacent to the measurement location for point FU7. (a) Location of structural damage at level 0.0 m, the yellow dot is damage to the wall structure, and the blue color is damage to the floor structure. The area marked with a red box is structural damage close to point FU8. (b) Cracks in the wall structure and some cracks have been repaired with concrete injection [3].

Figure 16 presents anomalies in the building vulnerability index (K_{tgj}) across several floor levels, indicated by significant differences exceeding 5.00 index units between the NS and EW wave components. These anomalies are observed at elevations of 32.25 meters (Figs. 16a and 16e), 17.40 meters (Figs. 16d and 16e), 13 meters (Fig. 16b), 8 meters (Figs. 16c and 16e), 0 meters (Figs. 16a-16c and 16e), and -6.50 meters (Figs. 16a-16b and 16d-e). The difference values range from 6.816 to 59.440. These variations are likely attributed to vibration noise generated by the reactor's support systems, which remained operational during the microseismic recordings. The directional dominance of these vibrations either in the NS or EW components may have influenced the seismometer readings at each measurement point.

CONCLUSION

This study investigated the structural characteristics of the reactor building and staircase building at the RSG-GAS facility, evaluating the main seismic and geotechnical parameters. The subsurface conditions at Serpong Nuclear Complex (SNC) and the RSG-GAS reactor showed significant variations in fundamental frequency (f_0), amplitude (A_0), and vulnerability index (K_g), indicating differences in soil response at various measurement points with the result that the building structure condition was at a low value for potential risk.

The resonance index values highlighted different structural behaviors, with some points categorized as medium class (FU1, FS9, and FB19) and high class (FS11). The inter-level deviation remained below the critical threshold at all points, indicating that the structural integrity of both buildings was within safe limits.

However, PGA analysis showed that most of the measurement points exceeded the critical limit, except for FU8, which recorded a value below the threshold. The building vulnerability index further identifies critical zones where structural sensitivity is most pronounced, specifically at FU1, FU7, and FS15 for the NS wave component, and FU1, FU8, FS15, and FS14 for the EW wave component. Overall, while the reactor building and staircase maintain stability within acceptable safety limits, certain zones exhibit higher vulnerability. These findings underscore the need for targeted structural assessments and potential strengthening strategies to improve resilience to seismic activity.

ACKNOWLEDGMENT

The researcher would like to express his deepest gratitude to the BRIN Degree By Research scholarship for the invaluable support and scholarship. Thanks were also expressed to the Director and employees of DPFK-BRIN for their assistance, especially in the Reactor RSG-GAS. Their contribution as research subjects is very important for the successful implementation of this research.

AUTHOR CONTRIBUTION

All authors read and approved the final version of the paper.

REFERENCES

1. I. P. Susila, A. Yuniarto and C. Cahyana, Atom Indones. **43** (2017) 87. (in Indonesian)
2. IAEA, IAEA Safety Standards: Seismic Hazards in Site Evaluation for Nuclear Installations, No. SSG-9, IAEA, Vienna (2010) 80.
3. S. Pujiarta, P. Busono, A. Azis *et al.,* Report on the Results of the Structural Strength Examination of the G.A. Siwabessy Reactor Building, National Nuclear Energy Agency, Serpong (2019) 1. (in Indonesian)
4. Y. Sanjaya, Majalengka's Baribis Fault Could Cause Earthquakes Like Cimandiri's Cianjur Fault, Here's the Explanation. https://radarcirebon.disway.id/read/145458/sesar-baribis-majalengka-bisa-gempa-darat-seperti-sesar-cimandiri-cianjur-begini-penjelasannya. Retrieved in February (2023). (in Indonesian)
5. United States Geological Survey, Earthquake Hazard Program - Search Earthquake Catalog.. https://earthquake.usgs.gov/earthquakes/search/. Retrieved in February (2023).
6. National Earthquake Center, Earthquake Map Book 2017, Ministry of Public Works and Housing Indonesia, Jakarta (2017) 1. (in Indonesian)
7. A. M. Al-Amri, K. Abdelrahman and M. S. Fnais, Arabian J. Geosci. **15** (2022) 1.
8. P. C. Basu, Nucl. Eng. Des. **352** (2019) 110140.
9. BAPETEN, Power Reactor Site Evaluation for Geotechnical Aspects and Power Reactor Foundations, BAPETEN Chairman's Regulation No. 4 of 2008, BAPETEN (2008). (in Indonesian)
10. Herak, *Recent applications of ambient vibration measurements in Croatia*, in Increasing Seismic Safety by Combining Engineering Technologies and Seismological Data, NATO Science for Peace and Security Series C: Environmental Security, United States (2008) 281.
11. M. Herak, Geofiz. **28** (2011) 21.
12. M. A. Hadianfard, R. Rabiee and A. Sarshad, Struct. Eng. Mech. **55** (2015) 965.
13. IAEA, IAEA Safety Standard: Safety Classification of Structures, Systems and Components in Nuclear Power Plants, No. SSG-30, IAEA, Vienna (2014) 1.
14. IAEA, IAEA Safety Standard: Evaluation of Seismic for Exixting Nuclear Installations, No. NS-G-2.13, IAEA, Vienna (2009) 1.
15. IAEA, IAEA Safety Standards Series: Seismic Design and Qualification for Nuclear Power Plants, No. NS-G-1.6 (2003) 1.
16. IAEA, IAEA Safety Standard: Ageing Management for Research Reactors, No. SSG-10 (Rev. 1), IAEA, Vienna (2023) 1.
17. Y. Nakamura, E. D. Guler and J. Saita, *Dynamic characteristics of leaning tower of pisa using microtremor*, 25th Japan Conference on Earthquake Engineering (1999) 921.
18. M. A. Hadianfard, M. Jahangiri and S. Shojaei, Soil Dyn. Earthquake Eng. **162** (2022) 107492.
19. M. Jahangiri, M. A. Hadianfard and S. Shojaei, Meas. **201** (2002) 111750.
20. P. Dunbar, H. McCullough, G. Mungov *et al.,* Geomatics Nat. Hazards Risk **2** (2011) 305.
21. Y. Nakamura, *Method for Dynamic Characteristics Estimation of Subsurface using Microtremor on the Ground Surface*, in: Quarterly Report of Railway Technical Research Institute Vol. No.1, Japan (1989) 25.
22. H. Arai and K. Tokimatsu, Bull. Seismol. Soc. Am. **95** (2005) 1766.
23. M. Khanmohammadi, M. Eshraghi, S. Behboodi *et al.,* J. Earthquake Eng. **26** (2021) 6015.
24. K. Konno and T. Ohmachi, Bull. Seismol. Soc. Am. **88** (1998) 228.
25. Y. Nakamura, E. D Gurler, J. Saita *et al., Vulnerability Investigation of Roman Colosseum using Microtremor,* 12th World Conference on Earthquake Engineering NZ 2660/6/A (2000) 1.

26. S. S. Arifin, B. S. Mulyatno, Marjiyono *et al.,* Jurnal Geofisika Eksplorasi **2** (2014) 30. (in Indonesian)
27. Daryono, Jurnal Kebencanaan Indonesia **2** (2009) 456. (in Indonesian)
28. Saaduddin, Sismanto, and Marjiyono, Proc. Seminar Nasional Kebumian **8** (2015) 459. (in Indonesian)
29. M. D. Trifunac and M. I. Todorovska, Soil Dyn. Earthquake Eng. **19** (2000) 253.
30. M. R. Gallipoli, M. Mucciarelli, S. Gallicchio *et al.,* Earthquake Spectra **20** (2004) S81.
31. E. Haghshenas. P. Y Bsard, N. Theodulidis *et al.*, Bull. Earthquake Eng. **6** (2008) 75.
32. M. Mucciarelli, M. R. Gallipoli and M. Arcieri, Bull. Seismol. Soc. Am. **93** (2003) 1407.
33. A. Gosar, Nat. Hazards Earth Syst. Sci. **10** (2010) 761.
34. A. Gosar, J. Rošer, B. Š. Motnikar *et al.*, Bull. Earthquake Eng. **8** (2010) 571.
35. M. Rudiger, M. Julian and S. Jurgen, *Design and Construction of Nuclear Power Plants*, Ernst & Sohn, Berlin (2013) 1.
36. BSN, Earthquake resistance planning procedures for building and non-building structures, 1726:2019 SNI, BSN, Jakarta (2019) 1. (in Indonesian)
37. T. Sato, Y. Nakamura and J. Saita, *The Change of the Dynamic Characteristics using Microtremor*, The 14th World Conference on Earthquake Engineering (1999) 12.
38. European Commission - Research General Directorate, Guidelines For the Implementation Technique on Ambient Vibrations of the H/V Spectral Ratio Technique on Ambient Vibrations, Project No. EVG1-CT-2000-00026 SESAME, European Commission - Research General Directorate, Brussels (2004) 62.
39. E. R. Iswanto, Y. Indrawati and T. A. Riyanto, Eksplorium **40** (2019) 105. (in Indonesian)
40. K. Kanai and T. Tanaka, Bull. Earthquake Res. Inst. **39** (1961) 97.
41. R. Prastowo and U. N. Prabowo, Angkasa Jurnal Ilmiah Bidang Teknologi **9** (2017) 83. (in Indonesian)
42. M. Zuhdi, M. Taufik, S. Ayub *et al.,* Introduction to Geophysics, Einstein College, Mataram (2021) 1. (in Indonesian)
43. Interatom, Construction Document of Civil Reactor RSG-GAS (Limited Document), Interatom, Bergisch Gladbach (1983) 1.